Quantification of source uncertainties in Seismic Probabilistic Tsunami Hazard Analysis (SPTHA)
Appendix A: Details in SPTHA assessments

J. Selva, R. Tonini, I. Molinari, M. M. Tiberti, F. Romano, A. Grezio, D. Melini, A. Piatanesi,, R. Basili, S. Lorito

Table of Contents

A.1 Basic input data

Several sources of information are available to characterize the seismicity and the seismo-tectonic settings of the selected application area and they are described in the following sub-sections.

A.1.1 Earthquakes

In each tectonic region (Fig. 3, main text), all the available information from catalogues is used for the quantifications relative to LEVELS 1, 2, and the BS- branch. In particular, seismicity catalogues are here used for defining: (i) the frequency-size distributions at LEVEL 1; (ii) the separation between IS and BS at LEVEL 2; (iii) the spatial distribution of BS events at LEVEL BS-1.

The European-Mediterranean Earthquake Catalogue (EMEC) provides location, epicentral intensity and magnitude of the seismic events for the last millennium (1000 – 2006) (Grünthal *et al.* 2010; Grünthal & Wahlström 2012). The EMEC compilation is based on 37 polygons that often follow national borders and within which the moment magnitudes Mw from the local catalogues are harmonized. The tectonic regions emerging from the regionalization (see A.2.1) do not correspond to the EMEC polygons. However, the completeness magnitude in the EMEC polygons may be associated to one or more tectonic regions (Tab. A1), in which we considered also additional information derived from Sørensen et al (2012) (for the Dead Sea Fault and Eastern Italy). Gutenber-Richter (GR) curves have been computed in each tectonic region to visually check the consistency of the association, for all magnitude levels and corresponding years in Tab. A1. In Fig. A1, we report the case of magnitude 4.5.

Table A1: Magnitude of completeness in the EMEC regions extracted for the tectonic regions of Fig. 1 (main text).

Magnitude	3.5	4.0	4.5	5.0	5.5	6.0	6.5	7.0	7.5	8.0	
***EMEC* Regions**											**Tectonic Regions**
Albania		1980	1970	1963	1920	1855	1830	1700			34
Apennines			1950	1875	1780	1400	1400	1000			25-28
Greece			1963	1963	1910	1910	1700	1500	1500	1400	7-13-23-29-30-31-35-40
Magreb		1950	1950	1920	1920	1870	1700	1700	1700		18-43
SouthApennines/Calabria			1900	1840	1820	1750	1550	1550			1-5-12-26-46
Sicily			1960	1910	1910	1750	350	350			14
Turkey West		1975	1970	1960	1900	1900	1600	1600	1200	1200	6
West Mediter. Sea			1975	1900	1900	1900					4
Sørensen et al. (2012)											
Eastern Italy	2006	1900	1900	1820	1220	1220	1100				17

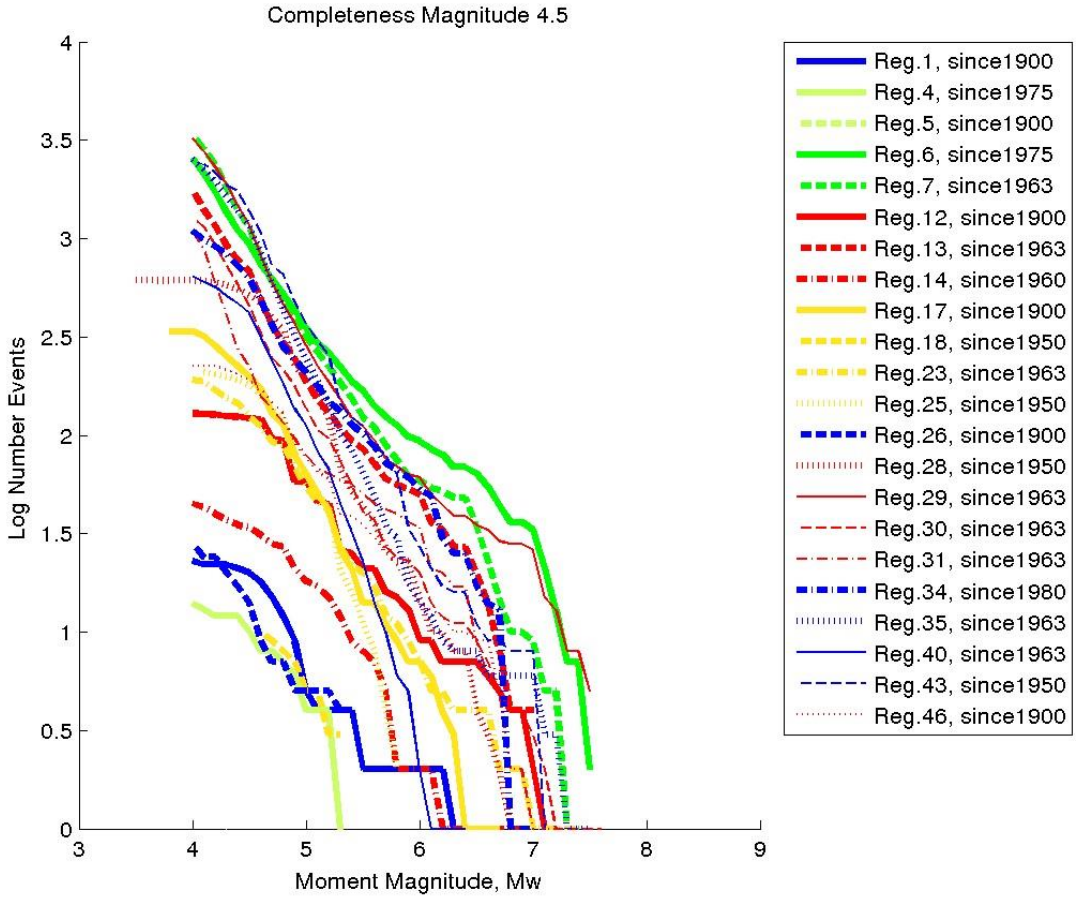

Figure A1. Cumulative frequency-magnitude curves of each tectonic region using the EMEC catalog. The completeness magnitude is 4.5 for all regions, while the relative completeness years are indicated for each region in the legend.

A.1.2 Focal mechanisms

The focal mechanism catalogues are essential at LEVEL BS-3 to define the potential faulting mechanism of the crustal events in each region, that is, for constraining BS faulting mechanisms.

A.1.2.1 AllCMT: Global Centroid-Moment Tensors and Regional Centroid-Moment Tensors

The AllCMT catalogue merges data from the Global Centroid Moment Tensor (GCMT) catalogue (Dziewonski et al, 1981; Ekström et al, 2012) and the Regional Centroid Moment Tensor (RCMT) catalogue (Pondrelli et al, 2002; Pondrelli et al, 2004; Pondrelli et al, 2006; Pondrelli et al, 2007; Pondrelli et al, 2011). Events with moment magnitude Mw > 5.5 are extracted from the GCMT and events with Mw ≤ 5.5 from the RCMT. The final dataset spans the temporal interval 1976-2013 (Pondrelli, personal communication). AllCMT events with hypocentral depth shallower than 30 km have been used.

A.1.2.2 EMMA: Earthquakes Mechanisms of the Mediterranean Area

The Earthquakes Mechanisms of the Mediterranean Area (EMMA) database (Vannucci and Gasperini, 2003; Vannucci and Gasperini, 2004; Gasperini and Vannucci, 2003) collects the focal solutions in published literature over the period 1905-2014 (unpublished version - October 2014; Vannucci 2015, personal communication). If multiple solutions exist for the same event, a flag indicates the preferred solution. This option allows users to avoid duplicate extractions of a selected solution.

A.1.3 Faults

The fault database is initially used to aid outlining the regionalization (see A.2.1) and then used at LEVEL BS-3 to define the potential faulting mechanism of the crustal events in each region.

The geometry and behavior of faults are taken from the EDSF (Basili et al., 2013). The subduction zones are defined by complex 3D geometry of the slab. The crustal faults have simple constant-dip geometry and behavior defined by rake (sense of movement), slip rate, and maximum magnitude. Although the database was specifically developed for a PSHA project (EU project SHARE, Woessner et al., 2015), it also contains information for several of the largest offshore faults in the Mediterranean Sea.

A.2 Tectonic framework

A.2.1 Regionalization

The main goal of the tectonic regionalization is to provide a framework for establishing the occurrence of the most likely faulting styles, guiding the selection of appropriate fault scaling laws, and estimating the seismicity rates by sampling the earthquake catalogues within tectonically homogeneous regions.

For the classification of tectonic regions (Fig. 3, main text, and Tab. A2), a first order subdivision is made between subduction zones and crustal regions. This is necessary in order to take separately into account the tectonic deformation occurring at a subduction plate boundary and the tectonic deformation occurring within the plate interiors. Tectonic deformation occurring at non-subduction plate boundaries (e.g. continental collision) is assimilated to crustal deformation.

Table A2: Regionalization nomenclature for the area in Fig. 3 (main text).

ID	Name	Category	Kinematics
1	Calabrian Arc North	Active region	Contraction
2	Hellenic Arc East	Active region	Contraction
3	Mediterranean Sea W	Stable oceanic region	Stable
4	Tyrrhenian Sea	Stable oceanic region	Extension
5	Ionian Sea	Stable oceanic region	Stable
6	North Anatolia	Active region	Fast strike slip
7	Kefalonia-Lefkada	Active region	Fast strike slip
10	Cyprian Arc	Subduction	Contraction
12	Calabria	Active region	Extension
13	Corinth	Active region	Extension
14	Sicily Channel	Stable continental region	Extension
16	Corsica Sardinia	Stable continental region	Stable
17	Adriatic	Stable continental region	Stable
18	Africa West	Stable continental region	Stable
20	Anatolia	Stable continental region	Stable
22	Macedonia	Active region	Extension
23	Africa East	Stable continental region	Stable
25	Tyrrhenian Sea	Stable continental region	Extension
26	Calabrian Arc	Subduction, Accretionary wedge	Contraction
28	Northern and central Apennines	Active region	Extension
29	Aegean South	Active region	Extension
30	Aegean Volcanic Arc	Active region - volcanic	Extension
31	Aegean North	Active region	Extension
34	Albanides - Hellenides	Active region	Contraction
35	Hellenic Arc	Subduction, Accretionary wedge	Contraction
39	Dinarides	Active region	Contraction
40	Hellenic Arc	Subduction, Accretionary wedge	Contraction
41	Northern and central Apennines	Active region	Contraction
43	Northern Africa	Active region	Contraction
46	Southern Apennines	Active region	Extension

A.2.1 Subduction

Subduction zones are complex tectonic systems made up by several features. Here, we use a simplified representation of the subduction which considers only the uppermost surface of the slab as the seismically active interface. The data are taken from EDSF (Basili et al., 2013a) which exploited several sources of information about the western Mediterranean lithospheric structure. We use two different representations: 1) depth contours for selecting earthquakes focal depth; 2) triangular meshing derived from the depth contours, for building individual rupture scenarios. The two representations are geometrically coherent and only serve the two different practical purposes.

Important definitions in the description and usage of the subduction zones are:

1. 'Nucleation' (seismogenic) zone: the part of the subduction interface where the earthquake rupture centers (or barycenters) are positioned.
2. 'Propagation' zone: the part of the subduction interface outside the seismogenic zone where earthquake ruptures can be allowed to "propagate". No earthquake rupture centers are allowed here. Note that we don't really simulate rupture propagation, as the ruptures are assumed to occur instantaneously and contemporarily over the fault plane. This serves only to assess rupture area used for simulations.
3. The acronym STEP, in the next two sections only, stands for Subduction-Transform Edge Propagator following the definition by Govers and Wortel (2005), not to be confounded with the word STEP used in the main text to discriminate the four stages of the hazard procedure proposed in this work.

A.2.1.1 Calabrian Arc subduction interface (Fig. A2a, LEVEL 2 and IS-branch)

Nucleation zone: The upper limit is taken at the first significant slab dip angle change (c. 10 km) and the lower limit at the second slab dip change (c. 40 km). The lateral limits are set to coincide with the NNW-SSE STEP fault offshore the eastern Sicilian coast, to the SW; and the approximate transition from the oceanic to continental crust to the NE.

Propagation zone: The upper limit is set at depths compatible with the presence of shallow splay faults cutting through the accretionary wedge and avoiding that the rupture top depth exceeds the seafloor depth. The lower limit is set at 10 km below the nucleation zone. The lateral limit to the SW is set to coincide with the same limit of the seismogenic zone. To the NE the limit is set farther away from the seismogenic zone, toward the significant strike change through the gradual transition to the Apennines continental collision in the Gulf of Taranto.

A.2.1.2 Hellenic Arc subduction interface (Fig. A2b, LEVEL 2 and IS-branch)

Nucleation zone: The upper limit is taken at the first significant slab dip angle change (c. 17 km) and the lower limit at a depth near the base of the most seismically active zone (c. 50 km) according to Heuret et al. (2011). The lateral limits are set to coincide with the NE-SW, STEP fault of the Ionian Islands (Kephallonia-Lefkada shear zone), and the gradual transition to decoupling/transcurrence East of Crete, where also the strike, dip, and rake, are very different from the rest of the arc.

Propagation zone: The upper limit is set at depths compatible with the presence of shallow splay faults cutting through the accretionary wedge and avoiding that the rupture top depth exceeds the seafloor depth (c. 15 km). The lower limit is set at 10 km below the nucleation zone. The lateral limit to the NW is set to coincide with the same limit of the seismogenic zone. To the E the limit is set farther away of the Rhodes Island toward the actual termination of the arc.

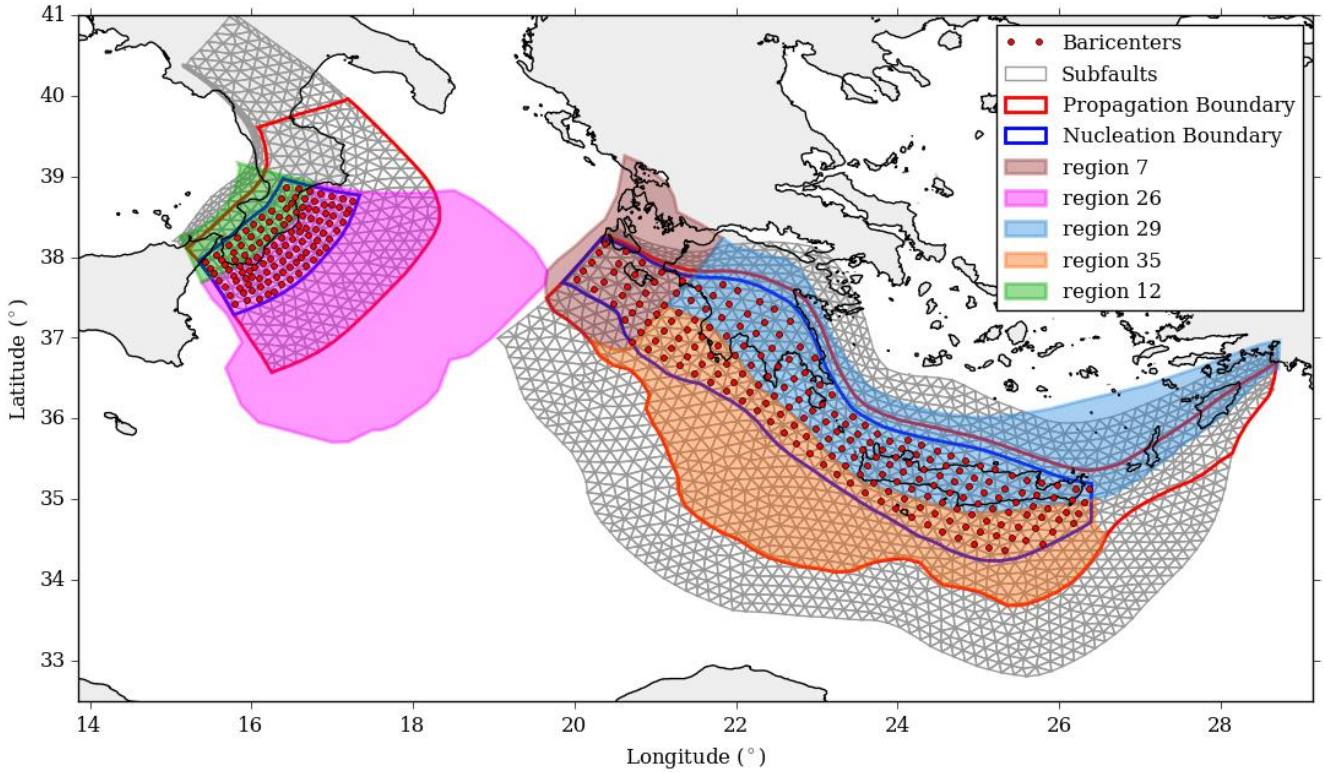

Figure A2 - Representation (mesh of triangular elements) of the two subduction zones of the Calabrian and Hellenic Arcs. Red dots are the geometrical centers of the earthquake ruptures used to spatially explore the slab interface. The blue and red polygons represent the boundaries of the nucleation and propagation zones, respectively. The color-shaded polygons are the various crustal regions (BS) overlapping the subduction interfaces and which are considered in various combinations with the relevant subduction for the calculation of earthquake occurrence rates.

A.2.2 Crustal regions

The main categories into which crustal regions are subdivided are as follows: stable continental, stable oceanic, and active. Active regions are further subdivided into three categories, representing the predominant tectonic regime such as contraction, extension, and transcurrence. Notice that transcurrence, or strike-slip faulting, may also significantly affects areas of either contraction or extension. The contractional regions also include deformation occurring within accretionary wedges associated with the upper plate in subduction zones. The map information is augmented by also outlining the presence of volcanic features.

For outlining the regions we use geologic and tectonic information derived from various large-scale, publicly available, maps and databases, such as the International Geological Map of Europe (IGME 5000; Asch 2005); the crustal models CRUST 1.0 (Laske et al. 2013) and EPCRUST (Molinari and Morelli, 2011); as well as datasets of peculiar features such as volcanoes (Siebert and Simkin 2002), ocean floor ages (Müller et al. 2008), plate boundaries (Bird 2003), and seismogenic faults from the European Database of Seismogenic Faults and local studies (EDSF; Basili et al., 2013a; Basili et al., 2013b; and references therein).

A.2.2.1 Discretization of the crustal domain (Fig. A3, BS-branch)

The crustal domain is further discretized into a regular grid (Fig. A3). The grid is composed by non-conformal equal-area cells of 25x25 km (cell sides depart from right angles with increasing distance from the origin; cell area is preserved everywhere). Elevation is taken from ETOPO2 (http://www.ngdc.noaa.gov/mgg/global/etopo2.html) as the average of all points within each grid cell. The grid has been generated considering all geographic coordinates in Lat/Lon, Datum WGS84, positive N/E, and a grid origin 29°N - 17°E.

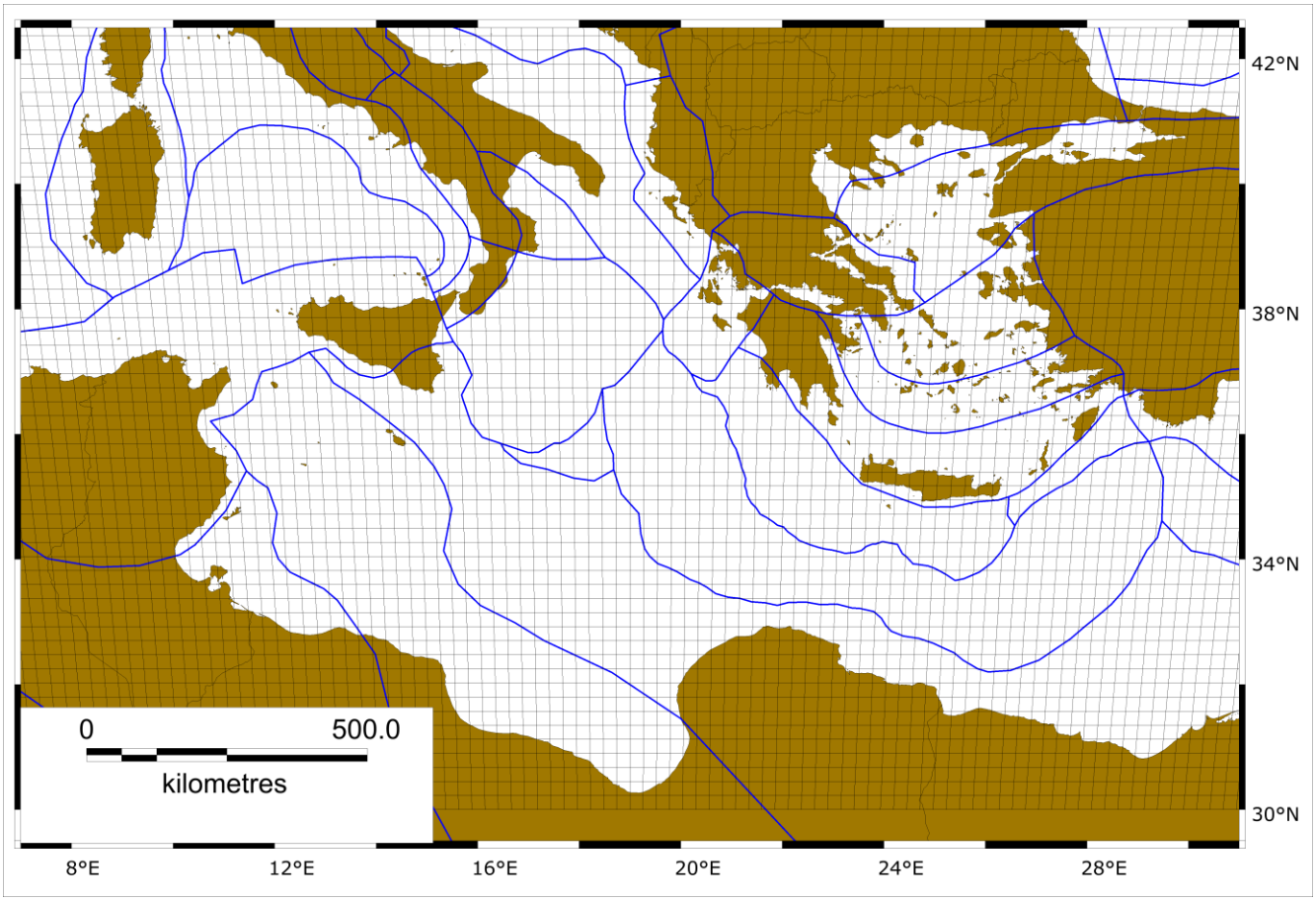

Figure A3 - The grid adopted at LEVELS B1-B2 and B3: it is composed by non-conformal equal-area cells of 25x25 km^2 (see text, for more details).

A.3 Probabilistic assessments for the Event Tree in each region

A.3.1 LEVEL 1: annual rates of magnitudes (Figs A4 and A5)

The alternative tree for LEVEL 1 is reported in Fig. A4. We end up with 3*2*2*2*2=48 alternative assessments with different weights, obtained by multiplying the weights at each branch. In particular:

- for λ *(m > 4.5)*, as starting data, we considered the observed episodes of exceedance each single year in the complete part of the EMEC catalog for magnitudes greater than 4.5. From this data, a Maximum Likelihood Estimation is adopted, considering 3 alternatives: the best guess (weight = 8), and the minimum and the maximum for a 0.95 confidence interval (both with weight = 1). In this way, we model a large variability of λ *(M > 4.5)*, in particular for low seismicity macro-regions;
- for Φ, we considered either Tapered Pareto (weight=3) or Truncated Pareto (weight=2);
- for β, we considered either 2/3 (corresponding to a b-value of 1 for a GR, weight=3) or computed from data (weight=7). The latter is actually not performed if less than 5 data are available in the catalog for the region. When this is true, only the first option is adopted;
- for the Tapered Pareto, we set in first approximation the corner magnitude M_c equal to M_{max}. Then, for both Tapered and Truncated Pareto, for M_{max} we consider:
    - for BS, either 7.5 or 8.0, equally weighted;.
    - for IS, either 8.8 or 9.1, equally weighted.

The resulting λ (M_i) for 2 macro-regions are reported in Fig. A5. Note that one macro-region contains two actual regions (#12 and #14), to completely include the Calabrian arc.

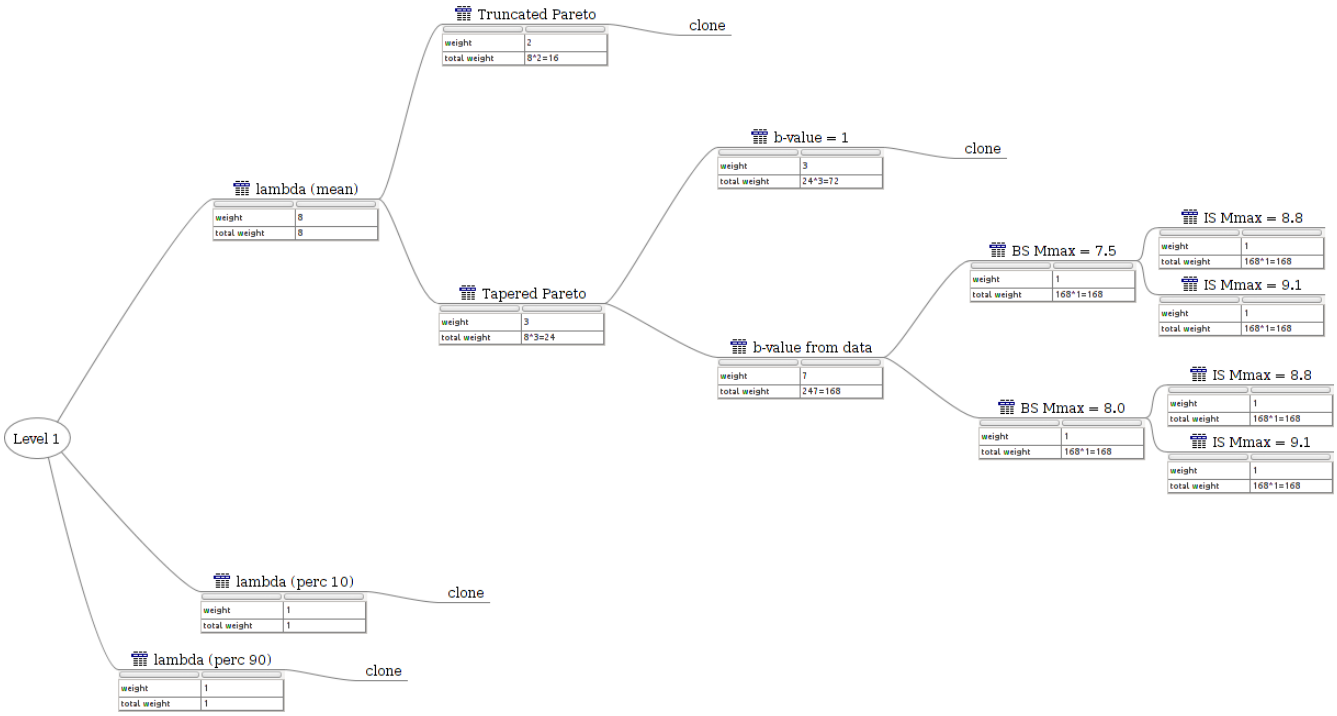

Figure A4: Alternative Tree for LEVEL 1. To simplify the graphics, we reported all the branches only in few cases, while the sub-tree structure is substituted with "clone" in all the other cases.

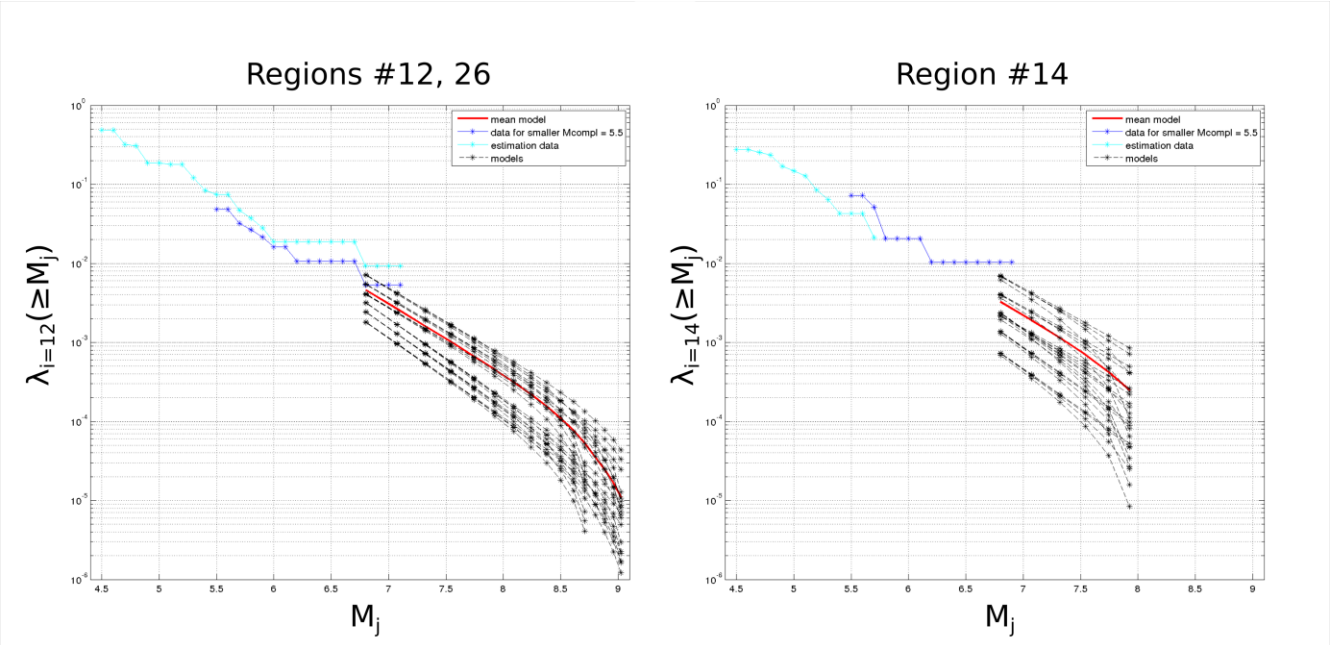

Figure A5: Resulting cumulative frequency size distributions, for the 48 alternative models in two randomly selected macro-regions (the macro-region of the Calabrian arc, containing regions #12 and #26, and region #14). The distributions are compared with the estimation data (light blue, completeness level of 4.5), the data from the same catalog with a completeness level of 5.5 (dark blue), and with the mean model (red).

A.3.2 LEVEL 2: probability of the different seismicity classes (Figs A6 and A7)

The alternative tree for LEVEL 2 is reported in Fig. A6. We end up with 12 alternative assessments with different weights obtained by multiplying the weights at each branch. In particular:

- for M_f, we consider two alternative choices: 5 and 6, with equal weights. If there are no events for M_f = 6 (as in the Calabrian arc) in the catalog, we just consider M_f=5;
- for counting nIS, only the events with a defined depth are considered; we adopted 5 alternative choices for the depth buffer around the subduction interface: 0, 5 km, 10 km, 15 km, ∞. The first and the last choices are implemented only for the sensitivity test, and thus they are reported here with weight=0. The 3 intermediate choices are equally weighted. Note that, in the case of infinity buffer, all events are modeled in the IS, and no BS is assumed everywhere (also in the regions not containing a subduction interface).
- for $f(x)$, $x>0$, we consider either linear or exponential function between M_f, that is

Linear:
$$f(M - M_f) = \begin{cases} \frac{M-M_f}{8-M_f} & for\ M < 8 \\ 1 & for\ M \geq 8 \end{cases} \quad \text{(B.1)}$$

Exponential:
$$f(M - M_f) = \begin{cases} \frac{\exp(M-M_f)}{\exp(8-M_f)} & for\ M < 8 \\ 1 & for\ M \geq 8 \end{cases}$$

The 2 alternative choices are equally weighted.

The resulting $\lambda^{IS}(M_i)$ and $\lambda^{BS}(M_i)$ for the macro-regions containing the Wester Hellenic arc and for the one containing the Calabrian arc are reported in Fig. A7, and compared to the observed data for the alternative buffers of 5, 10 and 15 km.

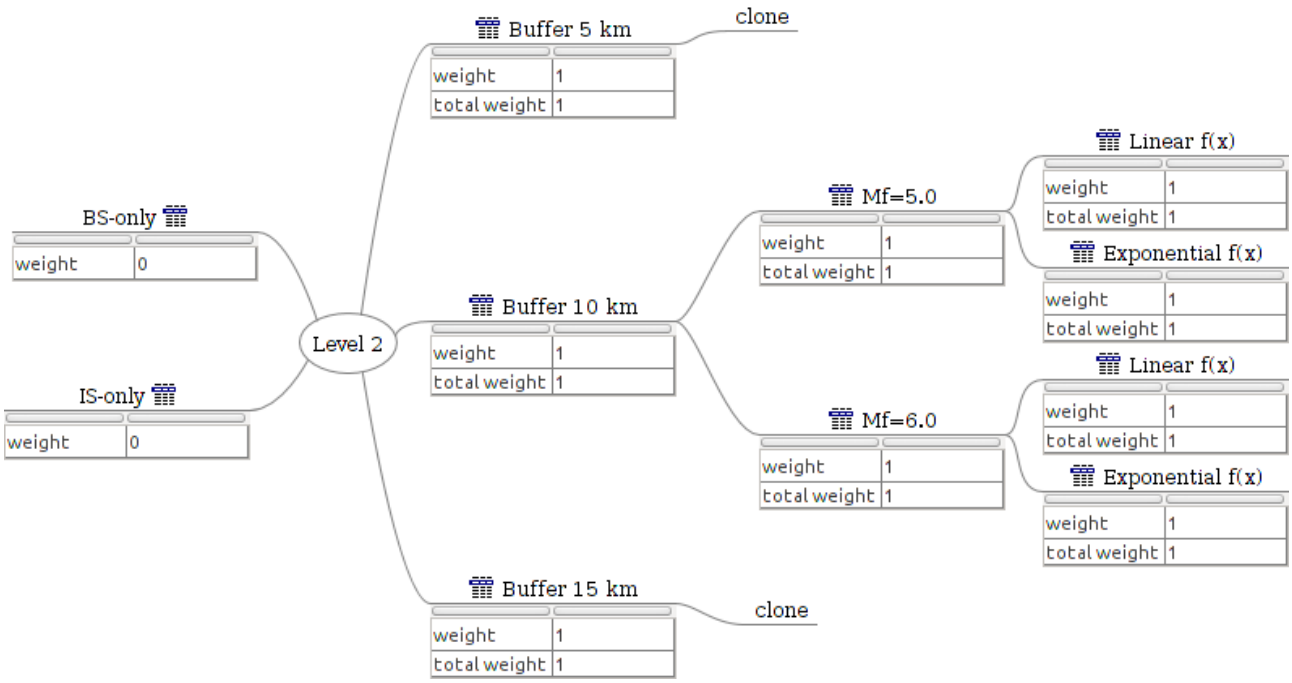

Figure A6: Alternative Tree for LEVEL 2. To simplify the graphics, we reported all the branches only in few cases, while the sub-tree structure is substituted with "clone" in all the other cases.

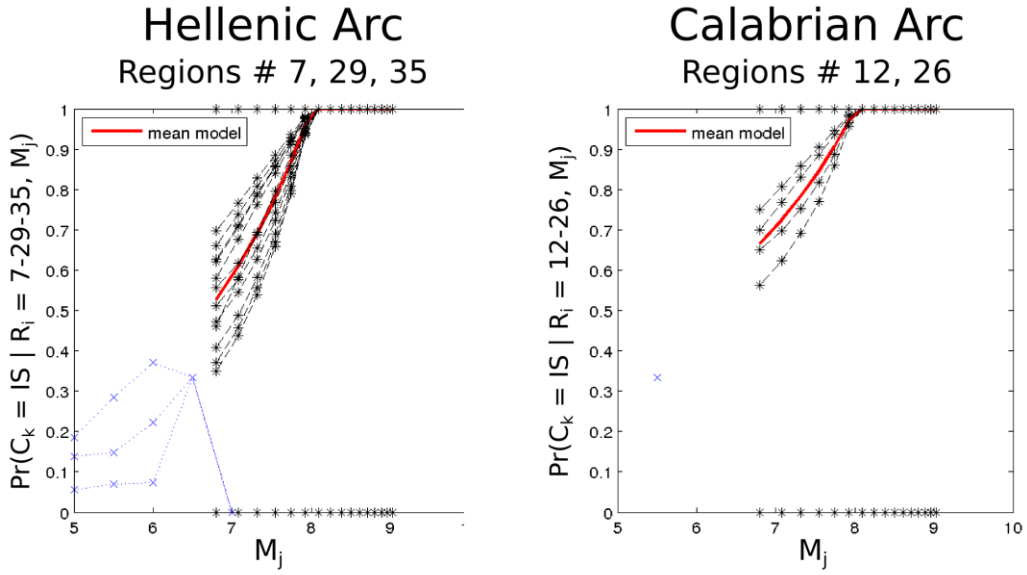

Figure A7: Resulting frequency of IS events with respect to BS evens, for the 12 alternative models. The functions are compared with the data for the 3 depth buffers (blue), when data are available, and with the mean model (red). Note that in many cases (for the largest magnitudes) less than 5 events are present, so the plotted points are not significant.

A.3.3 LEVEL BS-1: spatial probability of potential fault centers (Fig. A8)

Each center *x,y* of the grid (section A.2.2.1, Fig. A3) is considered as potential central point for earthquakes. Two alternatives are considered for LEVEL BS-1, a uniform distribution and a smoothed seismicity, with weights 3 and 2 respectively. In both cases, M > 4.5 are considered. We consider only the BS events emerging from LEVEL 2, meaning that, in the macro-regions in which the subduction interface is present, the two alternatives are combined with the 5 alternative models considered at LEVEL 2 (buffers = 0 km, 5 km, 10 km, 15 km, and ∞), obtaining a total of 2*5=10 theoretical alternatives, of which only 2*3=6 are effectively explored through the alternative tree (buffer = 0 and and ∞ have both weight 0). Note that the case buffer = ∞ implies no events within the BS seismicity class, leading to a probability 0 of BS seismicity everywhere (only IS seismicity is modelled in this case). The smoothed seismicity is computed only if more than 50 events are present in the region. In the case of uniform distribution, the probability of each center is simply obtained by counting the number of centers within each region n_c, and assigning to each one of them a probability of $1/n_c$. The smoothed seismicity is computed adopting the parameterization proposed in Hiemer et al. (2014), with dc=10 km and n=2 (kernel distance and number of nearest-neighbors, respectively), considering that the same database is considered here, and for simplicity only the most recent time interval of completeness is considered. The spatial event distribution for all regions, multiplied by the mean model for annual rates of exceedance of M=4.5, is reported in Fig. A8. Note that, in several regions, the two alternative models coincide, since not enough events (50) are present in the catalog. For simplicity, only the case of buffer equal to 5 km is reported in figure: no significant differences are observed for the other buffers of 0, 10 and 15 km.

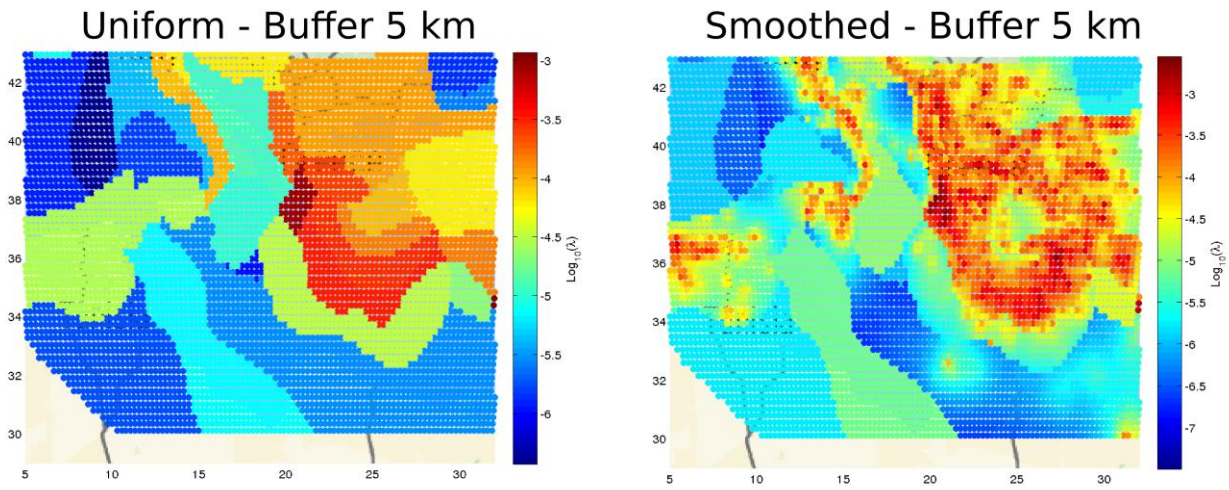

Figure A8: spatial distribution for the whole region, multiplied by the mean model for mean annual rates of exceedance of M=4.5, for two alternative models: a uniform distribution in each region (left panel) and smoothed seismicity (right panel), both computed from a depth buffer of 5 km at LEVEL 2. Note that, if less than 50 events are found in the area, a uniform distribution is adopted also in the smoothed seismicity branch.

A.3.4 LEVEL BS-2: probability of potential depths of the fault centers

For BS, depth is discretized in a number of intervals that depends on the magnitude level, and in particular, the number of interval is set as

$$n_i = ceiling\left(\frac{W_s - W(M_i)/\sqrt{2} - 1}{W(M_i)/2\sqrt{2}}\right), \quad \text{(B.2)}$$

where W_s is the width of the seismogenic zone and $W(M_i)$ is the most likely width (mean) of crustal faults for a magnitude M_i, computed adopting Wells and Coppersmith (1994). In particular, the depth intervals (corresponding to the centers of the modeled faults) are set uniformly distributed from a minimum depth equal to $W(M_i)/2+1$ km to a maximum depth of $Ws - W(M_i)/2$ (in both cases, the average sea bottom depth is referred to the cell (x,y)). In this way, the number of intervals is set so that the spacing along z is equal to fault width (along the vertical) when a dip angle of 45 degrees is assumed. The value of Ws has been fixed to 27 km, accordingly to the average crustal thickness in the entire considered domain derived from the CRUST 1.0 model (Laske et al. 2013). The results for the different magnitude levels are reported in Tab. A3. In case of BS-only, we adopted an alternative discretization. Since the IS-branch contribution is missing, all cells belonging to regions in subduction zones (see Fig. 3, main text) are treated differently: we extend the range of magnitudes up to 9.026 and we set the seismogenic boundary to 50 km, in order to consider also the interplate events. The resulting discretization is shown in Tab. A4. No alternative models are implemented in both cases.

Table A3: Number of depth intervals used for all cells for BS, with the exception of the case BS-only.

Mw	n_i	Depth values (km)
6.8012	5	6.188, 10.093, 14.000, 17.907, 21.814
7.0737	4	7.339, 11.780, 16.220, 20.661
7.3203	3	8.602, 14.000, 19.398
7.5435	2	9.961, 18.039
7.7453	2	11.398, 16.602
7.9280	1	12.896

Table A4: Number of depth intervals and values used for cells belonging to regions in subduction zones for BS-only assessment.

Mw	n_i	Depth values (km)
6.8012	9	6.186, 11.015, 15.843, 20.672, 25.500, 30.328, 35.157, 39.985, 44.814
7.0737	7	7.339, 13.393, 19.446, 25.500, 31.554, 37.607, 43.660
7.3203	6	8.602, 15.361, 22.120, 28.880, 35.639, 42.398
7.5435	5	9.961, 17.731, 25.500, 33.269, 41.039
7.7453	4	11.398, 20.799, 30.201, 39.602
7.9280	4	12.896, 21.299, 29.701, 38.104
8.0933	3	14.437, 25.500, 36.563
8.2429	3	16.003, 25.500, 34.997
8.3782	2	17.576, 33.424
8.5007	2	19.142, 31.858
8.6115	1	20.685
8.7118	1	22.195
8.8025	1	23.660
8.8846	1	25.073
8.9588	1	26.426
9.026	1	27.716

A.3.5 LEVEL BS-3: probability of the potential faulting mechanisms (Fig. A9)

At LEVEL BS-3, we adopted the same Bayesian inference procedure using two input catalogs: AllCMT and EMMA (see A.1 for details on these catalogs). These two catalogs represent the two alternative implementations at this LEVEL, with weight 3 for the catalog AllCMT and weight 2 for EMMA. As for LEVEL BS-1, also at this LEVEL we use only the BS events emerging from LEVEL 2 meaning that, in the regions in which the subduction interface is present, each branch of the alternative tree is duplicated for all the potential depth

buffer sizes at LEVEL 2 (0, 5, 10, and 15 km). Since the case buffer = ∞ implies a probability identically 0 everywhere at LEVEL BS-1, this alternative has not to be implemented here.

To assess the probability of occurrence for all faulting mechanisms, canonical strike and dip angles are first transformed according to Selva and Marzocchi (2004), that is

$$\begin{cases} S = strike \\ D = dip \end{cases} \quad for\ 0 \geq strike > 180 \qquad \text{(B.3)}$$

$$\begin{cases} S = strike - 180 \\ D = 180 - dip \end{cases} \quad for\ 180 \geq strike > 360$$

This transformation is adopted so that two sub-vertical faults (e.g., dip = 89) with two complementary strikes (e.g., strike = 30 and 210) will result close in the parameter space (in this case, S=30 and D=89 and 91, respectively). Then, the discretization is made in the parameter space {S, D, rake}. In particular:

- 4 S intervals for strike: [0,45[, [45,90[, [90,135,[135,180[, centered in 22.5,66.5,112.5, and 157.5
- 9 D intervals for dip: [0,20[, [20,40[, [40,60[, [60,80[, [80,100[, [100,120[, [120,140[, [140,160[, [160,180[, centered in 10, 30, 50, 70, 90, 110, 130, 150, 170
- 4 rake intervals: [-135,-45[,[-45,45[,[45,135,[135,180] U [-180,-135[, centered in -90, 0, 90, +/-180

As first guess prior, a semi-informative prior is adopted to exclude unlikely faulting mechanisms. In particular:

- For rake centered in -90 (normal faults), we exclude (Pr=0) D centered in 10, 90 and 170;
- For rake centered in 0 or +/-180 (strike-slip faults), we exclude (Pr=0) D centered in 10, 30, 50, 130, 150, and 170;
- For rake centered in 90 (inverse faults), we exclude (Pr=0) D centered in 70, 90 and 110;

We name the remaining intervals I_p, which will be the only ones possible in the posterior. For these intervals, a uniform distribution with maximum epistemic uncertainty (equivalent number of data equal to 1, see Selva et al. 2012) is set. This prior distribution is updated by considering either the AllCMT or the EMMA catalog (see Appendix A.1.2), assigning weights to these alternative catalogs of 3 and 2, respectively. Each catalog contains the estimation of two auxiliary fault planes. Given that we do not know which one is the true plane for each earthquake, when either of the two auxiliary planes are theoretically possible (considered the prior distribution set) both planes are included as past data, weighting by ½ each one of them, modelling in this way the uncertainty on the data (e.g., Selva and Sandri 2013). Following this procedure, we obtain a posterior distribution in the form of a Dirichlet distribution with parameters:

$$\alpha_k^{(region)} = \delta_{k,p}^{prior} + \delta_{k,p}^{prior} \cdot \sum_j \left\{ \frac{\delta_{kj}^{(1)}}{2} + \frac{\delta_{kj}^{(2)}}{2} \right\}$$

where $\delta_{k,p}^{prior}$ is 1 if the k-the interval is among the possible ones, 0 otherwise; $\delta_{kj}^{(1)}$ is 1 if the first focal plane is in the *k*-th interval, 0 otherwise; $\delta_{kj}^{(2)}$ is 1 if the second focal plane is in the *k*-th interval, 0 otherwise. Note that, the contribution of past data (in bracket) is suppressed if one event lies outside the intervals I_p. Indeed, these potential events are considered not possible in the prior, so this datum (if present) is assumed to be wrong.

This Dirichlet distribution represents the state of knowledge regarding the possible faulting planes for all the cells (*x,y)* in one region. If known faults exist in one particular cell, then this information is used to update the parameters of the regional distribution, since they represent an important piece of information to be considered regarding potential faulting mechanisms. In particular, following Selva et al. (2010), a new prior model is produced by considering the geologic fault mechanisms, with an equivalent number of data (equivalent sample size) equal to 100. Since this equivalent number of data is much larger than the one adopted for the regional prior, this information will tend to lead in the cell. If two or more faults are present in the same cell, we weight the geologic fault mechanisms of the known faults by the *log10* of their known moment rate (as a proxy for their relative seismic productivity). This leads to

$$\alpha_k^{(cell)} = \begin{cases} \alpha_k^{(region)} \\ \alpha_k^{(region)} + \sum_m w_m \delta_{mk} \end{cases}$$

where $w_m = \dot{M}_m / \sum_l \dot{M}_l$ and δ_{mk} is equal to 1 if the mechanism of the faults is in the *k*-th interval, and 0 otherwise. Since no data are considered at the cell level, the final model is represented by a Dirichlet distribution with parameters $\alpha_k^{(cell)}$. If no faults are known in a cell, the regional model is instead considered, with parameters $\alpha_k^{(region)}$.

The Bayesian procedure allows a simultaneous assessment of the aleatory and epistemic uncertainty. Therefore, for each one of the *Ns* sampled alternative simulations, first we sampled which catalog has to be used (either AllCMT or EMMA), then we sample from the posterior Dirichlet distribution, obtaining a statistical mixing of the two alternative models relative to the two input catalogs (for more details, see Selva et al. 2014, Tonini et al. 2015). In macro-regions containing more than one region, the sampled model for LEVEL 2 is adopted for filtering the dataset.

In Fig. A9, we report the results of the mean of the posterior distribution for region #7. This region is part of the macro-region relative to the Western Hellenic arc, thus the total number of alternatives is 8 (4 buffers at LEVEL 2 and 2 alternatives at this LEVEL). The results do not vary dramatically depending on the buffer, while relatively higher variations are observed between the two source catalogs.

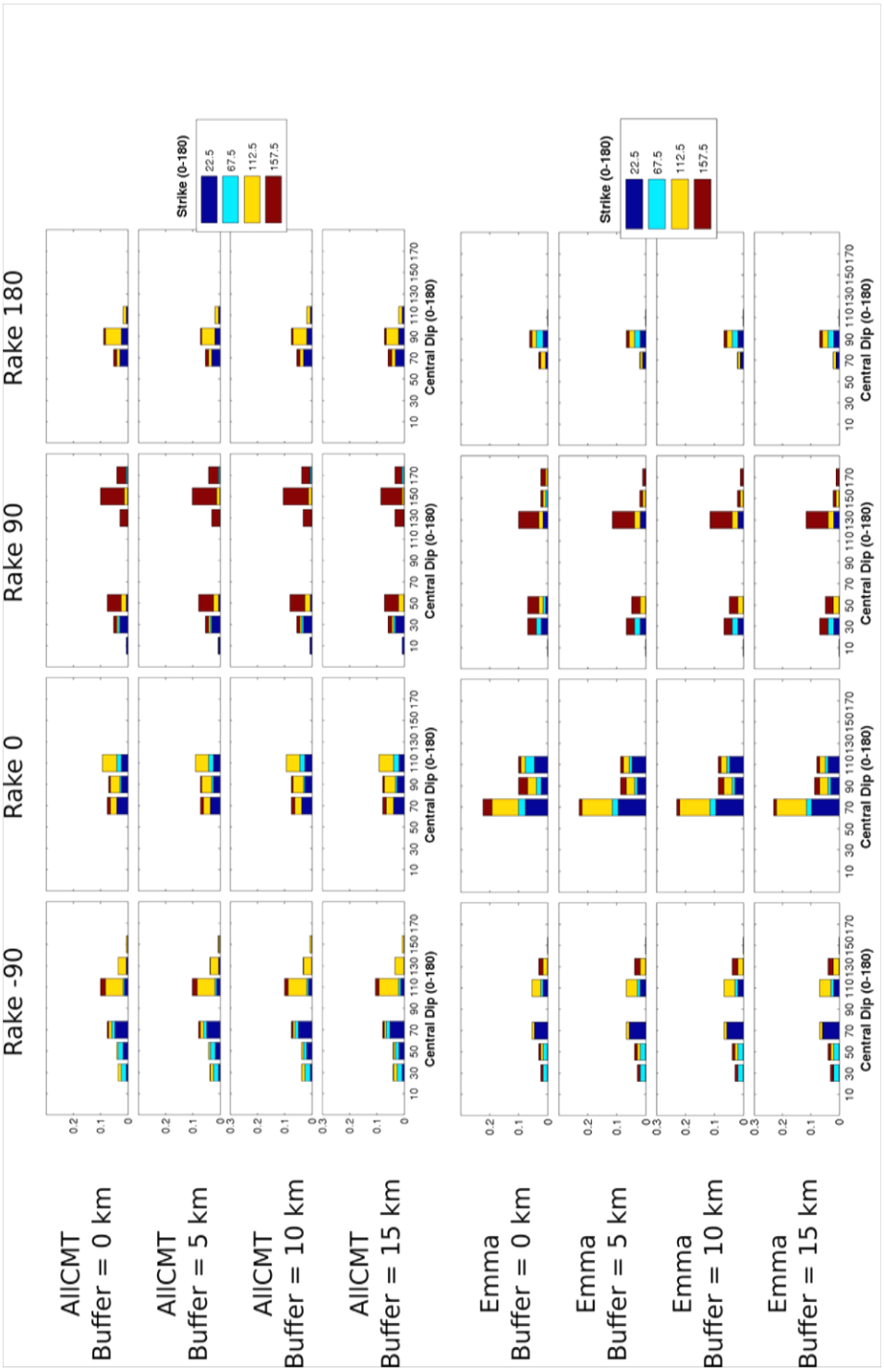

Figure A9: Mean values of the posterior distribution for the region #7. The results are reported for all the combinations of depth buffer for LEVEL 2 (excluding ∞) and the alternatives at LEVEL BS-3 (4x2=8 rows, from up to down, we consider buffers of 0, 5 km, 10 km and 15 km with catalog AllCMT first, then for Emma). In the different columns, we group the results for the different rake intervals (from left to write, centered in -90, 0, 90, 180).

A.3.6 LEVELS BS-4 and BS-5: probability for the maximum rupture area and seismic moment distribution along each finite fault

Here, for simplicity, we disregard the variability of the rupture area around its best guess value and potential heterogeneities in moment and mechanism distribution at the LEVEL BS-4. In particular, for the rupture area *A* we assume as only possible value the best guess of the scaling laws for crustal seismicity (no distinction is made for the different angles) presented in Wells and Coppersmith (1994). At LEVEL BS-5, only a uniform value of rigidity μ of 30 GPa is assumed, so that the slip results uniform in direction and modulus over the rupture area A. No alternative models are implemented at these LEVELS.

A.3.7 LEVELS IS-1 and IS-2: probability of the possible position of fault centers and maximum rupture area and seismic moment distribution along each finite fault

At LEVEL IS-1, we divide the interface into a nucleation zone (at classical seismogenic depths), and a propagation zone (a larger area around the boundaries of the nucleation zone), as reported in Fig. A2 and discussed in section A.2.1. We implement two alternative models for LEVEL IS-1: we either force the event to remain within the nucleation zone, or we allow it to extend to the propagation zone, with weights 2 and 3 respectively. For each potential earthquake's barycentre (red dots in Fig. A2) and each magnitude, we calculate the theoretical maximum rupture area of a rectangular shape fault by means of scaling laws (Strasser et al., 2010). Then we find the subset of triangular elements which represents at best these shape and area. When the theoretical rectangular area is not fully contained in the slab (since the barycentre is located close to slab's boundaries or the earthquake is very large) we adapt systematically the shape to the slab's morphology, preserving the total area. However, not all the earthquakes are considered as possible and the following rejection criteria are adopted:

1. at least 25% of the theoretical rectangular fault is not contained in the slab's boundary;
2. the theoretical area is too large with respect the area of the whole slab (≥10%);
3. the theoretical area and the area of the corresponding best selection of triangular elements differ more than ±10%.

Of course, when propagation is allowed, the center of faults can be much closer to the border of the nucleation area, so that the uniform moment release is extended to a greater area, while the probability that the propagation zone be involved in the coseismic rupture increases with the size of the earthquake. Note that this is just a first attempt of modeling the propagation of large energetic ruptures into weaker zones, e.g. the trench zone, as for the 2011 Tohoku earthquake. Of course, different implementations are possible. Note that this implementation likely barely allows for "tsunami earthquakes", at it is not possible to have events that slips mainly in the propagation zone.

As in LEVEL BS-5, at LEVEL IS-2 only a uniform value of rigidity μ of 30 GPa is assumed, so that the slip results uniform in direction (pure thrust) and modulus over the rupture area A.

No alternative models are implemented at these LEVELS. However, we note that in a real assessment it will be important to model moment (slip) variability over the finite faults, and possibly consider some shallow slip amplification, especially for IS seismicity and in the near-field of the targets.

A.4 Disaggregation results at higher intensity levels (Figs A10-A13)

In this paragraph, we report the results of the disaggregation of the hazard for the target points, considering levels of the intensity of 3 and 5 m, for comparison with the analogous results reported in the main text for an intensity level of 1 m (Figs 9 and 10, main text).

In Figs A10 and A11, we report the disaggregation for regions at tsunami intensities of 3 and 5 m, respectively. It can be noted that the general influence of the regions in the near-field (with only BS, reported in black) tends to increase, as the intensity level increases. At the same time, as the number of sources that may cause larger tsunamis diminishes, the impact of epistemic uncertainty on their rates tends to increase, resulting in larger error bars in Figs A10 and A11. Note also that in several cases, the mean values fall outside the error bars, indicating distributions highly asymmetric with fat tails toward large values.

In Figs A12 and A13, we report the disaggregation for cells at tsunami intensities of 3 and 5 m, respectively. In these plots, as in the main text, only the mean of the epistemic uncertainty is reported. It can be noted that the cells causing such large intensities tend to diminish in number, and to concentrate in the near-field with respect to the targets (red crosses in the figures). In addition, the propagation feature are even more marked for those higher intensities, since the number of influencing cells diminishes, and the propagation patterns of the remaining sources emerge clearer.

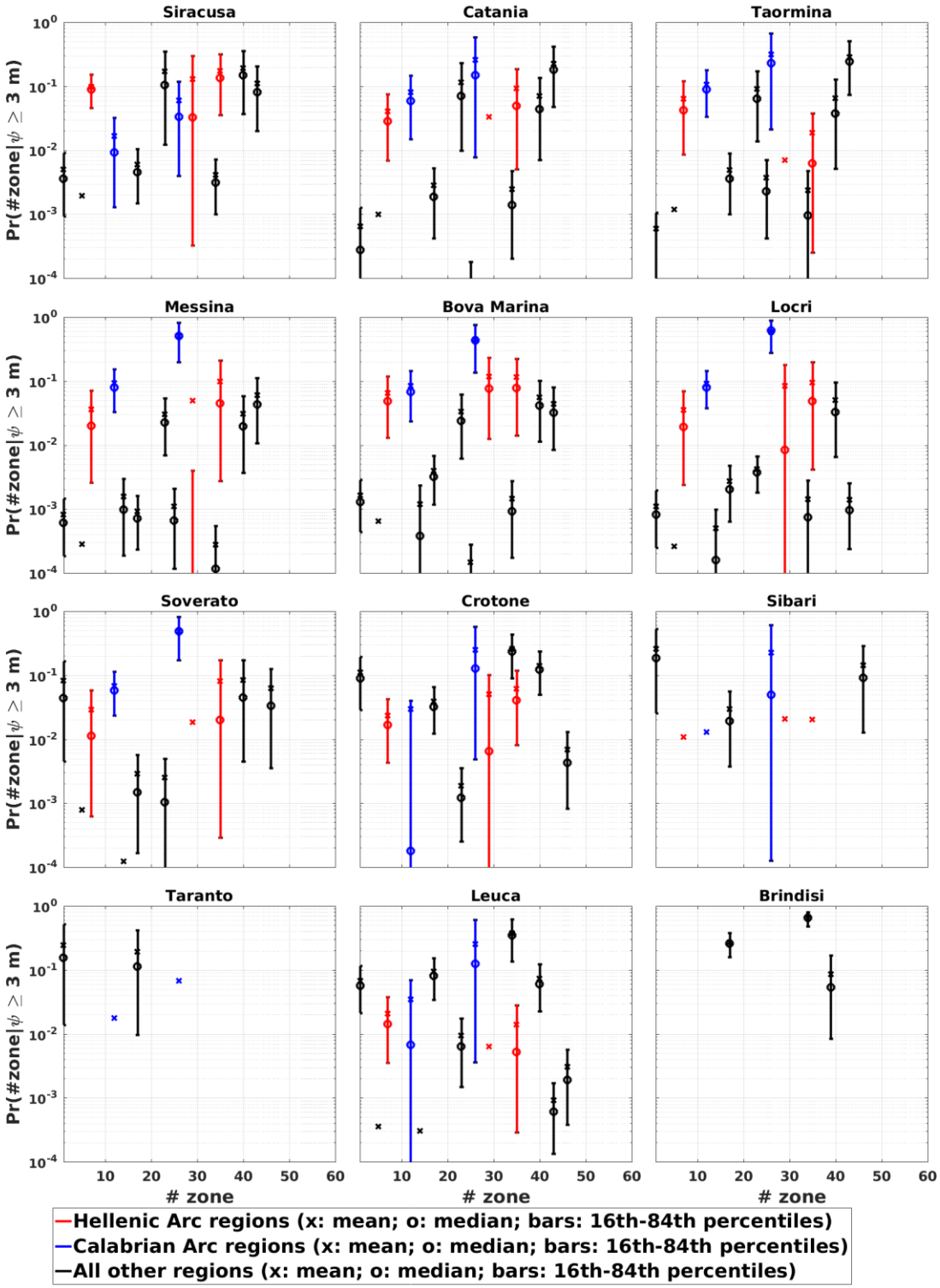

Figure A10: Region disaggregation results for an intensity threshold of 3 m. In the regions in which IS is present, both IS and BS contributions are considered.

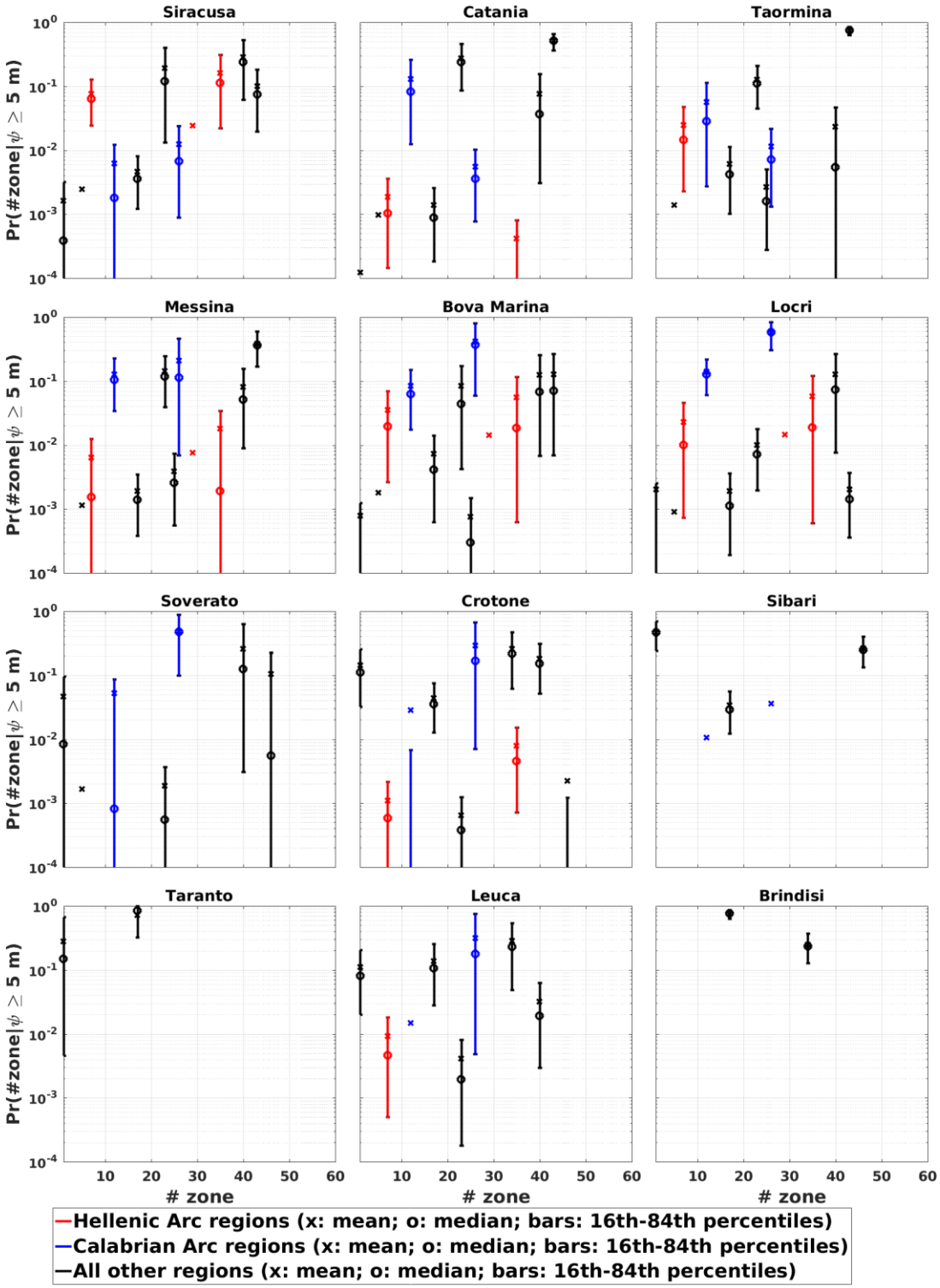

Figure A11: Region disaggregation results for an intensity threshold of 5 m. In the regions in which IS is present, both IS and BS contributions are considered.

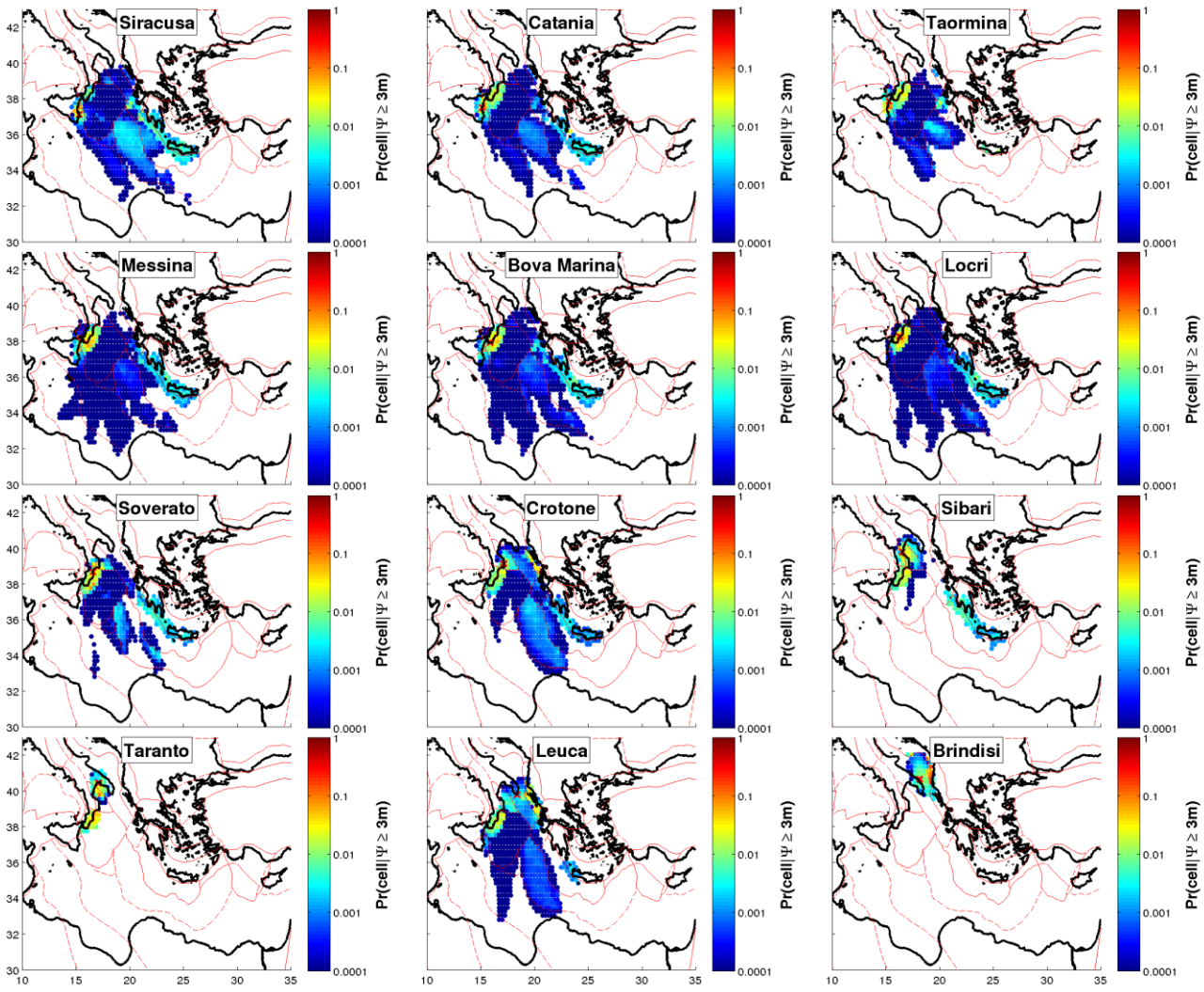

Figure A12: Cell disaggregation results for an intensity threshold of 3 m. In each cell, both IS and BS events with fault centers in each cell are considered. The red crosses report the locations of the target considered in each panel.

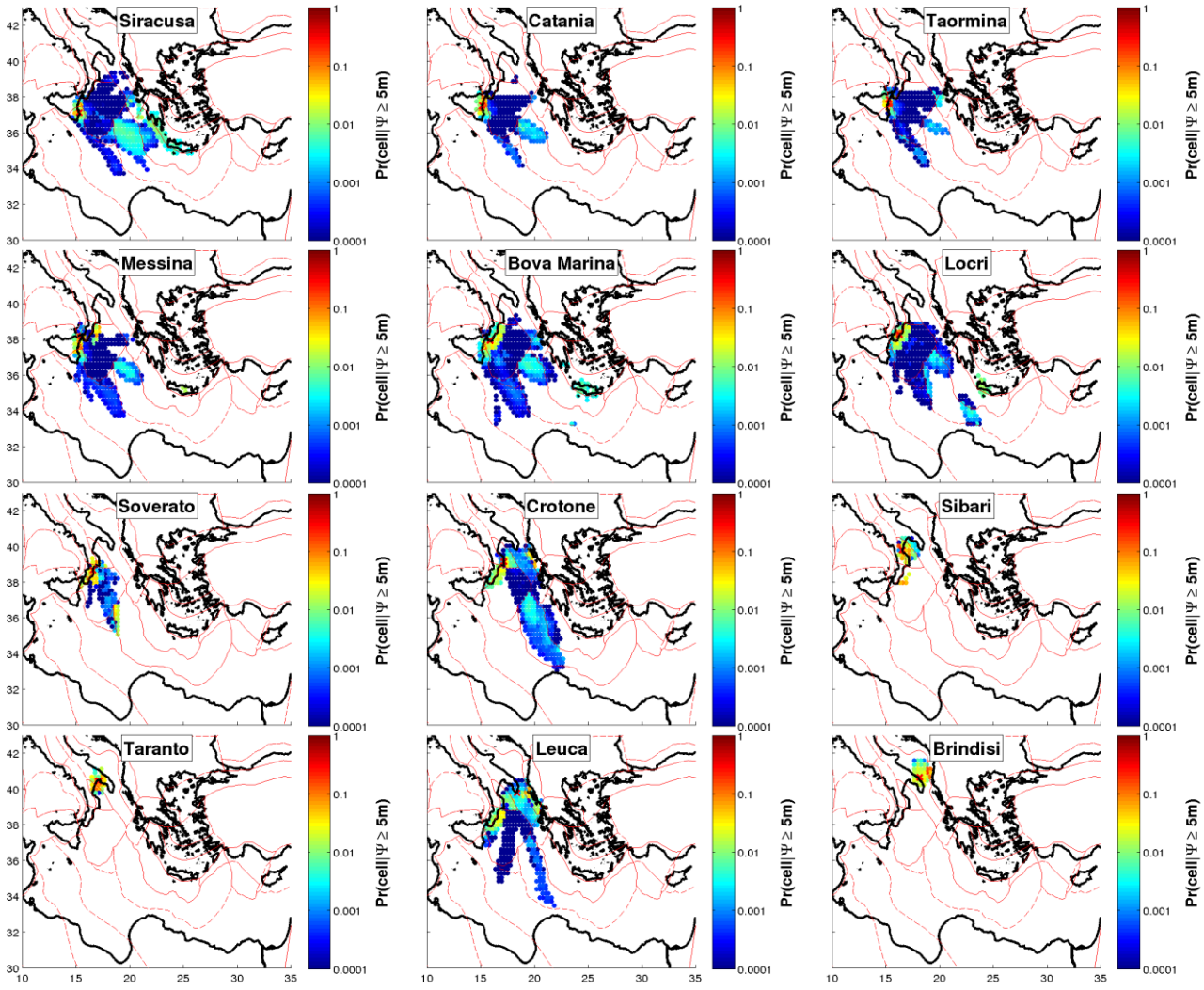

Figure A13: Cell disaggregation results for an intensity threshold of 5 m. In each cell, both IS and BS events with fault centers in each cell are considered. The red crosses report the locations of the target considered in each panel.

References

Asch, K., 2005. The 1:5 Million International Geologial Map of Europe and Adjacent Areas. In: BGR, Hann. http://www.bgr.de/karten/igme5000/igme5000.htm.

Basili R., Kastelic V., Demircioglu M. B., Garcia Moreno D., Nemser E. S., Petricca P., Sboras S. P., Besana-Ostman G. M., Cabral J., Camelbeeck T., Caputo R., Danciu L., Domac H., Fonseca J., García-Mayordomo J., Giardini D., Glavatovic B., Gulen L., Ince Y., Pavlides S., Sesetyan K., Tarabusi G., Tiberti M. M., Utkucu M., Valensise G., Vanneste K., Vilanova S., & Wössner J., 2013a. The European Database of Seismogenic Faults (EDSF) compiled in the framework of the Project SHARE. http://diss.rm.ingv.it/share-edsf/, doi: 10.6092/INGV.IT-SHARE-EDSF.

Basili, R., Tiberti, M.M., Kastelic, V Romano, F., Piatanesi, A., Selva, J., & Lorito, S., 2013b. Integrating geologic fault data into tsunami hazard studies, Nat. Hazards Earth Syst. Sci., 13, 1025–1050.

Bilek, S. L. & Lay, T., 1999. Rigidity variations with depth along interplate megathrust faults in subduction zones, Nature, 400, 443–446.

Bird, P., 2003. An updated digital model of plate boundaries. Geochemistry, Geophys Geosystems 4:n/a–n/a. doi: 10.1029/2001GC000252.

Dziewonski, A.M., Chou, T.-A., & Woodhouse, J.H., 1981. Determination of earthquake source parameters from waveform data for studies of global and regional seismicity, J. Geophys. Res. 86, 2825-2852

Ekström G., Nettles, M., & Dziewoński, A.M., 2012. The global CMT project 2004–2010: Centroid-moment tensors for 13,017 earthquakes, Physics of the Earth and Planetary Interiors, Volumes 200–201, June 2012, Pages 1–9, doi:10.1016/j.pepi.2012.04.002

Gasperini, P., Vannucci, G., 2003. FPSPACK: A package of simple FORTRAN subroutines to manage earthquake focal mechanism data, Computers & Geosciences, 29, 893-901.

Geist, E.L., & Bilek, S.L., 2001. Effect of depth-dependent shear modulus on tsunami generation along subduction zones. Geophysical Research Letters, 28: 1315–1318. doi: 10.1029/2000GL012385.

Govers, R., Wortel, M.J.R., 2005. Lithosphere tearing at STEP faults: response to edges of subduction zones, Earth Planet. Sci. Lett., 236, 505–523

Grünthal, G., Arvidsson, R., & Bosse, C., 2010. Earthquake Model for the European - Mediterranean Region for the Purpose of GEM1. Scientific Technical Report STR10/04

Grünthal, G., & Wahlström, R., 2012. The European - Mediterranean Earthquake Catalogue (EMEC) for the last millennium. Journal of Seismology, 16, 3, 535 - 570 DOI: 10.1007/s10950-012-9302-y

Heuret, A., Lallemand, S., Funicello F., Piromallo, C., Faccenna, C., 2011. Physical characteristics of subduction interface type seismogenic zones revisited, Geochem. Geophys. Geosyst., 12, Q01004, doi:10.1029/2010GC003230

Hiemer, S., Woessner, J., Basili, R., Danciu, L., Giardini, D., & Wiemer, S., 2014. A smoothed stochastic earthquake rate model considering seismicity and fault moment release for Europe, Geophys. J. Int,, Vol, 198, p. 1159-1172, doi:10.1093/gji/ggu186. doi:10.1016/S0031-9201(02)00214-5

Laske, G., Masters., G., Ma, Z., & Pasyanos, M., 2013. Update on CRUST1.0 - A 1-degree Global Model of Earth's Crust, Geophys. Res. Abstracts, 15, Abstract EGU2013-2658.

Meade, B.J., 2007. Algorithms for the calculation of exact displacements, strains, and stresses for triangular dislocation elements in a uniform elastic half space, Comput. Geosci. 33, 1064-1075, doi:10.1016/j.cageo.2006.12.003,

Molinari, I., & Morelli, A., 2011. EPcrust: a reference crustal model for the European Plate: Geophysical Journal International, v. 185, no. 1, p. 352-364, doi 10.1111/j.1365-246X.2011.04940.x.

Müller R.D., Sdrolias, M., Gaina, C., & Roest, W.R., 2008. Age, spreading rates, and spreading asymmetry of the world's ocean crust. Geochemistry, Geophys Geosystems 9:n/a–n/a. doi: 10.1029/2007GC001743.

Pondrelli, S., Morelli, A., Ekström, G., Mazza, S., Boschi, E., & Dziewonski, A.M., 2002. European–Mediterranean regional centroid-moment tensors: 1997–2000. Phys.Earth Planet Int. 130, 71–101.

Pondrelli, S., Morelli, A., & Ekström, G., 2004. European-Mediterranean regional centroid-moment tensor catalog: solutions for years 2001 and 2002. Phys. Earth Plan. Int., 145, 1-4, 127-147

Pondrelli, S., Salimbeni, S., Ekström, G., Morelli, A., Gasperini, P., Vannucci, G., 2006. The Italian CMT dataset from 1977 to the present Phys. Earth Planet Int., 159, pp. 286–303

Pondrelli, S., Salimbeni, S., Morelli, A., Ekstr¨ m, G., & Boschi, E., 2007. European-Mediterranean Regional Centroid Moment Tensor catalog: Solutions for years 2003 and 2004, Phys. Earth Planet.In., 164, 90–112, doi:10.1016/j.pepi.2007.05.004

Pondrelli S., Salimbeni, S., Morelli, A., Ekström, G., Postpischl, L., Vannucci, G., & Boschi, E., 2011. European–Mediterranean Regional Centroid Moment Tensor catalog: Solutions for 2005–2008 Physics of the Earth and Planetary Interiors, Volume 185, Issues 3–4, Pages 74–81

Selva, J., & Sandri, L., 2013. Probabilistic Seismic Hazard Assessment: Combining Cornell-like approaches and data at sites through Bayesian inference , Bull. Seism. Soc. Am., 103(3):1709-1722, DOI: 10.1785/0120120091

Selva, J., Costa, A., Marzocchi, W., & Sandri, L., 2010. BET_VH: exploring the influence of natural uncertainties on long-term hazard from tephra fallout at Campi Flegrei (Italy) , Bull. Volcanol. 72(6): 705-716.

Selva, J., Marzocchi, W., Papale, P., & Sandri, L., 2012. Operational eruption forecasting at high-risk volcanoes: the case of Campi Flegrei, Naples, J. Applied Volcanology 1:5, DOI:10.1186/2191-5040-1-5

Selva, J., Costa, A., Sandri, L., & Marzocchi, W., 2014. Probabilistic short-term volcanic hazard in phases of unrest: a case study for tephra fallout, J. Geophys. Res., 119(12): 8805-5526, DOI:10.1002/2014JB011252

Sørensen, M.B., Spada, M., Babeyko, A., Wiemer, S. & Grünthal, G., 2012. Probabilistic tsunami hazard in the Mediterranean Sea, J. geophys. Res., 117, B01305, doi:10.1029/2010JB008169

Siebert, L., & Simkin, T., 2002. Volcanoes of the World: an Illustrated Catalog of Holocene Volcanoes and their Eruptions. Smithsonian Institution, Global Volcanism Program Digital Information Series, GVP-3. http://www.volcano.si.edu.

Strasser, F.O., Arango, M.C., & Bommer, J.J., 2010. Scaling of the Source Dimensions of Interface and Intraslab Subduction-zone Earthquakes with Moment Magnitude, Seismological Research Letters, November/December 2010, v. 81, p. 941-950.

Tonini, R., Sandri, L., Costa, A., & Selva, J., 2015. Brief Communication: The effect of submerged vents on probabilistic hazard assessment for tephra fallout, Nat. Hazards Earth Syst. Sci., 15, 409-415, doi:10.5194/nhess-15-409-2015.

Vannucci, G., & Gasperini, P., 2003. A database of revised fault plane solutions for Italy and surrounding regions, Computers & Geosciences 29, 903-909.

Vannucci, G., & Gasperini, P., 2004. The new release of the database of earthquake mechanisms of the Mediterranean area (EMMA Version 2), Annals of Geophysics 47, 307-334.

Vannucci G., Imprescia, P., & Gasperini, P., 2010. Deliverable n. 2 of the UR2.05 in the INGV-DPC S1 project (2007-2009). INGV-DPC Internal report and database.

Wells, D.L. & Coppersmith, K.J., 1994. New Empirical Relationships among Magnitude, Rupture Length, Rupture Width, Rupture Area, and Surface Displacement, Bulletin of the Seismological Society of America, 84 (4), 974-1002.

Woessner J., Danciu L., Giardini D., Crowley H., Cotton F., Grünthal G., Valensise G., Arvidsson R., Basili R., Demircioglu M., Hiemer S., Meletti C., Musson R.W., Rovida A., Sesetyan K., Stucchi M., & the SHARE consortium, 2015. The 2013 European Seismic Hazard Model - Key Components and Results. Bulletin of Earthquake Engineering, doi: 10.1007/s10518-015-9795-1.